# Diverging volumetric trajectories following pediatric traumatic brain injury

Emily L. Dennis[a,*], Joshua Faskowitz[a], Faisal Rashid[a], Talin Babikian[b], Richard Mink[c], Christopher Babbitt[d], Jeffrey Johnson[e], Christopher C. Giza[f,i], Neda Jahanshad[a], Paul M. Thompson[a,g], Robert F. Asarnow[b,h,i]

[a] Imaging Genetics Center, Mark and Mary Stevens Institute for Neuroimaging and Informatics, Keck School of Medicine, University of Southern California, Marina del Rey, CA 90292, USA
[b] Department of Psychiatry and Biobehavioral Sciences, Semel Institute for Neuroscience and Human Behavior, UCLA, Los Angeles, CA 90024, USA
[c] Harbor-UCLA Medical Center and Los Angeles BioMedical Research Institute, Department of Pediatrics, Torrance, CA 90509, USA
[d] Miller Children's Hospital, Long Beach, CA 90806, USA
[e] LAC + USC Medical Center, Department of Pediatrics, Los Angeles, CA 90033, USA
[f] UCLA Brain Injury Research Center, UCLA Steve Tisch BrainSPORT Program, Dept of Neurosurgery and Division of Pediatric Neurology, Mattel Children's Hospital, Los Angeles, CA 90095, USA
[g] Departments of Neurology, Pediatrics, Psychiatry, Radiology, Engineering, and Ophthalmology, USC, Los Angeles, CA 90033, USA
[h] Department of Psychology, UCLA, Los Angeles, CA 90024, USA
[i] Brain Research Institute, UCLA, Los Angeles, CA 90024, USA

## ARTICLE INFO

## ABSTRACT

Traumatic brain injury (TBI) is a significant public health concern, and can be especially disruptive in children, derailing on-going neuronal maturation in periods critical for cognitive development. There is considerable heterogeneity in post-injury outcomes, only partially explained by injury severity. Understanding the time course of recovery, and what factors may delay or promote recovery, will aid clinicians in decision-making and provide avenues for future mechanism-based therapeutics. We examined regional changes in brain volume in a pediatric/adolescent moderate-severe TBI (msTBI) cohort, assessed at two time points. Children were first assessed 2–5 months post-injury, and again 12 months later. We used tensor-based morphometry (TBM) to localize longitudinal volume expansion and reduction. We studied 21 msTBI patients (5 F, 8–18 years old) and 26 well-matched healthy control children, also assessed twice over the same interval. In a prior paper, we identified a subgroup of msTBI patients, based on interhemispheric transfer time (IHTT), with significant structural disruption of the white matter (WM) at 2–5 months post injury. We investigated how this subgroup (TBI-slow, $N = 11$) differed in longitudinal regional volume changes from msTBI patients (TBI-normal, $N = 10$) with normal WM structure and function. The TBI-slow group had longitudinal decreases in brain volume in several WM clusters, including the corpus callosum and hypothalamus, while the TBI-normal group showed increased volume in WM areas. Our results show prolonged atrophy of the WM over the first 18 months post-injury in the TBI-slow group. The TBI-normal group shows a different pattern that could indicate a return to a healthy trajectory.

## 1. Introduction

Traumatic brain injury (TBI) can have lasting, devastating effects, especially in children whose brains have not fully matured. Some children fully recover, or experience only mild disability, while others experience profound disruption years post-injury. Injury severity is a factor in predicting outcome, but leaves considerable variance in outcome unexplained (Saatman et al., 2008). Our incomplete understanding of recovery prevents clinicians from caring for patients most effectively. Charting longitudinal changes in the brain post-injury is critical for determining how long-term disruption occurs in patients, and may identify targeted interventions, critical windows for such interventions, and clinically useful predictors. Here we examined longitudinal changes in regional brain volume following a moderate/severe TBI (msTBI) in pediatric/adolescent patients.

Group differences in injury severity, type, and location complicate analyses of brain trauma that involve inter-subject registration and group comparisons. MsTBI is associated with volumetric deficits in the

---

corpus callosum (CC), and across the gray and white matter in adults (Farbota et al., 2012; Kim et al., 2008; Sidaros et al., 2009) as well as ventricular enlargement (Kim et al., 2008). Subcortical volumetric deficits have been detected in children and adults (Farbota et al., 2012; Kim et al., 2008; Sidaros et al., 2009; Wilde et al., 2007). Additionally, the cerebellum, peduncles, and brainstem show deficits following a brain injury (Farbota et al., 2012; Sidaros et al., 2009). Numerous studies have investigated volumetric deficits in pediatric TBI patients (Levin et al., 2000; Wilde et al., 2007; Wu et al., 2010), and TBM has been used previously to study adult TBI patients (Farbota et al., 2012; Kim et al., 2008; Sidaros et al., 2009), but to our knowledge, our prior paper was the first applying TBM to pediatric/adolescent TBI (Dennis et al., 2016). In our prior paper, we examined msTBI patients cross-sectionally at 2–5 months and 13–19 months post-TBI for regional differences in brain volume. We found expansion of the lateral ventricles at both time points, and reduced volume in clusters throughout all lobes. Here we examined longitudinal changes in those msTBI children. Studies of longitudinal volume changes in adult TBI patients show progressive atrophy across the brain (Farbota et al., 2012; Sidaros et al., 2009). Longitudinal studies of volume change in pediatric patients have mostly focused on the corpus callosum, with msTBI associated with progressive decreases in callosal volume (Levin et al., 2000; Wu et al., 2010).

Tensor-based morphometry (TBM) is a sensitive method for assessing regional volume change that offers advantages over other volumetric approaches. Longitudinally, TBM generates deformation fields that track local volumetric growth and tissue loss, warping baseline anatomy to match a later scan (Hua et al., 2016; Thompson et al., 2000). The deformation fields indicate regions of volume expansion or contraction in an individual scan, showing changes from the first assessment. TBM analyzes the whole brain, surveying changes without requiring a priori hypotheses about where the changes occur, and without defining regions of interest. TBM does not rely on accurate segmentation of the gray/white matter tissue boundaries, as VBM (voxel based morphometry) does. Tissue segmentation can be problematic in heavily damaged brains.

We previously found a subset of patients within the msTBI group who have markedly poorer neural integrity (Dennis et al., 2015a). MsTBI patients were divided into two groups based on their interhemispheric transfer time (IHTT – the time to transfer information between right and left hemispheres) measured as an event-related potential (ERP) (Ellis et al., 2015). The msTBI group with longer IHTTs (TBI-slow) had poorer WM structural integrity and cognitive impairment relative to healthy controls. The msTBI group with normal IHTTs (TBI-normal), however, had few areas of disrupted WM structural integrity, with no significant cognitive impairment. These differences were not easily explained by demographic or clinical variables. In this paper we compared these three groups, testing for differences in longitudinal changes in regional brain volume. We hypothesized that the TBI-slow group would show greater longitudinal decreases in volume relative to the TBI-normal and control groups.

## 2. Materials and methods

### 2.1. Participants

TBI participants were recruited from four Pediatric Intensive Care Units (PICUs) located in Level 1 and 2 Trauma Centers in Los Angeles County. In these institutions, patients with msTBI are routinely admitted to the PICU. A study representative discussed the study goals with the parents of patients, gave them an IRB-approved brochure about the study and obtained permission for the investigators to contact them after discharge from the medical center. Parents additionally signed consent forms allowing access to medical records. IRB approval was obtained by each recruitment site. 35% of patients whose parents agreed to be contacted while the child was in the PICU participated in

this study. Out of 124 families contacted at the PICUs, 27 were lost to contact (kept canceling/rescheduling), 21 did not qualify because they did not meet criteria (GCS – Glasgow Coma Scale (Teasdale et al., 1979) – > 12, English skills not sufficient, ADHD,[1] learning disability, braces, etc.), 26 were not interested, and 50 are participating. Of these, not all have longitudinal data. 1 subject was scanned chronically, but data quality issues (artifacts) meant we could not include them, 3 subjects only received functional MRI at the chronic time point, 2 subjects were brought back for the chronic assessment but not scanned, 3 had braces at time 2, 3 were disqualified at time 2 for ADHD or LD (learning disability), 1 family refused to return, 2 moved out of state, 1 was referred by his doctor to the study and had already missed the post-acute window, and 8 were lost to follow-up, meaning they could have moved, changed their phone number, or simply stopped returning our calls. There was no systematic reason for the non-returns. Healthy controls, matched for age, sex, and educational level, were recruited from the community through flyers, magazines, and school postings.

#### 2.1.1. Inclusion criteria

1) non-penetrating msTBI (intake or post-resuscitation GCS score between 3 and 12); 2) 8–18 years of age at the time of injury; 3) right-handed; 4) normal visual acuity or vision corrected with contact lenses/eyeglasses; and 5) English skills sufficient to understand instructions and be familiar with common words (the neuropsychological tests used in this study presume competence in English).

#### 2.1.2. Exclusion criteria

1) history of neurological illness, such as prior msTBI, brain tumor or severe seizures; 2) motor deficits that prevent the subject from being examined in an MRI scanner (e.g., spasms); 3) history of diagnosed psychosis, ADHD, Tourette's Disorder, learning disability, mental retardation, autism or substance abuse. These conditions were identified by parental report and are associated with cognitive impairments that might overlap with those caused by TBI. Participants were excluded if they had metal implants that prevented them from safely undergoing a MRI scan.

Demographic information from our sample is consistent with existing epidemiological information on moderate-severe pediatric/adolescent TBI, both in the male to female ratio and in the types of mechanisms of injury (Keenan and Bratton, 2006). The injury mechanisms for our msTBI group were: 6 motor-vehicle accident (MVA) – pedestrian, 3 MVA – passenger, 6 fall – skateboard, 3 fall – scooter, 2 fall – bike, 1 fall – skiing, 1 assault, 1 uncategorized blunt head trauma. Information on all three groups can be found in Table 1.

### 2.2. Scan acquisition

Participants were scanned on 3 T Siemens Trio MRI scanners with magnetization-prepared rapid gradient echo imaging (MPRAGE). The T1-weighted images were acquired with the following acquisition parameters: GRAPPA mode; acceleration factor PE = 2; TR/TE/TI = 1900/3.26/900 ms; FOV = 250 × 250 mm; an axial plane acquisition with isotropic voxel size = 1 mm, flip angle = 9°.

### 2.3. Scan comparison

Part-way through the study, scanning moved from the UCLA Brain Mapping Center (BMC) to the Staglin IMHRO Center for Cognitive Neuroscience (Staglin). Both scanners were 3 T Siemens Trio scanners, and the protocol was maintained. To determine that this scanner change did not introduce bias into our data, we scanned 6 healthy adult volunteers at both the BMC and Staglin centers, 1.5 months apart. We then assessed possible bias in both the T1-weighted images and

---

[1] Attention Deficit Hyperactivity Disorder.

**Table 1**

Demographic information. We list the number of participants in the TBI-slow, TBI-normal, and control groups, the male/female ratio, the average age at both assessments (and standard deviation), the IHTT (inter-hemispheric transfer time, in ms), the TSI (time since injury, in weeks, average and standard deviation), and ICV (intracranial volume). We had acute CT information for all TBI participants, and these findings are summarized as well. SAH = subarachnoid hemorrhage, IVH = intraventricular hemorrhage, EDH = epidural hematoma, SDH = subdural hematoma, ICH = intracerebral hemorrhage, DAI = diffuse axonal injury, ICP ↑ = increased intracranial pressure, Dep FX = depressed skull fracture, ND FX = non-depressed skull fracture. These numbers do not include the 6 volunteers who were included to control for scanner change effects. The * indicates a statistically significant difference between group values.

|  | TBI-slow | TBI-normal | Control |
|---|---|---|---|
| N | 11 | 10 | 26 |
| M/F | 8/3 | 8/2 | 15/11 |
| IHTT avg. (SD) | 25.5 (6.3)* | 7.8 (5.5) | 10.4 (5.0) |
| Avg. age at T1 (SD) | 14.1 (1.9) | 16.0 (2.6) | 14.5 (3.0) |
| Avg. age at T2 (SD) | 15.0 (2.0) | 17.0 (2.8) | 15.6 (3.0) |
| Avg. ICV (SD) | 1955 (63) | 1902.9 (45.9)* | 1950 (61) |
| Avg. scan interval (SD) | 50.6 (5.9) | 52.5 (9.7) | 61.2 (10.3)* |
| Avg. GCS (SD) | 8.8 (3.6) | 9.4 (4.0) | – |
| SAH | 3 | 3 | – |
| SDH | 4 | 2 | – |
| IVH | 2 | 1 | – |
| EDH | 5 | 4 | – |
| ICH | 6 | 4 | – |
| DAI | 1 | 0 | – |
| Contusion | 5 | 3 | – |
| ICP | 1 | 2 | – |
| Dep Fx | 3 | 3 | – |
| ND Fx | 4 | 3 | – |

diffusion-weighted images. Extensive details of this process are found in our paper (Dennis et al., 2015b). For the T1-weighted images, the scan comparison analyses revealed no detectable pattern in the difference between the intensity correction fields above noise, except in the cerebellum, where some scanner induced differences in image intensity were detected even after N3 correction (intensity correction). For this reason, the cerebellum was masked out of the analyses presented in this paper.

### 2.4. Cognitive performance

Our cognitive performance score is a summary measure assessing multiple domains affected in TBI (Babikian and Asarnow, 2009). It is a linear, unit weighted combination of the following age-based standardized or scaled measures: 1) Processing Speed Index from the WISC-IV/WAIS-III (Wechsler, 2003); 2) Working Memory Index from the WISC-IV/WAIS-III (Wechsler, 2003); 3) Trials 1–5 from the CVLT-C/II (Delis et al., 1994); and 4) Trails 4 from the D-KEFS (Delis et al., 2001). Further details of our performance index are found in our prior paper (Moran et al., 2016).

### 2.5. Tensor-based morphometry

Each subject's T1-weighted anatomical data (both time points) was N3-corrected using c3d (http://www.itksnap.org) to correct for intensity inhomogeneities. Volumes were automatically skull-stripped using Brainsuite (http://brainsuite.org) and these masks were manually edited by trained neuroanatomical experts (ELD and FR). We linearly registered each subject to a study-specific template using *flirt* (http://fsl.fmrib.ox.ac.uk). We used a study-specific registration template, which can lead to better registration results (Hua et al., 2013). We chose a healthy control male, aged 14.2 (the average for our sample at time 1) with a visually normal T1-weighted scan to initialize the linear registration. This exemplar subject was registered to the ICBM template using the fsl tool *flirt* (http://fsl.fmrib.ox.ac.uk), using 7 degrees of freedom registration, with trilinear interpolation, and using mutual information as the similarity function for alignment. Following this,

each subject's masked, NU-corrected T1-weighted image was registered to the subject-template using iterative 6, 7, and 9 DOF registration. We concatenated transformation files so that only one resampling step was run. This protocol was modified for this dataset from the original protocol (Hua et al., 2009; Hua et al., 2008).

Next, each subject's template-aligned T1 from the chronic time point was non-linearly aligned to the template-aligned T1 from the post-acute time point, using the ANTs Symmetric Normalization (SyN; (Avants et al., 2008)). SyN registration used a multi-level approach, i.e., the "moving" and fixed T1 images were successively less smoothed at each level, with a full resolution registration occurring at the final level. We chose to use 150, 50, and 5 iterations at each level, with a Gaussian kernel smoothing sigma set to 3, 1, and 0 respectively (7.05, 2.35, and 0 voxels FWHM). Image similarity was measured using the ANTs implementation of mutual information (Avants et al., 2011).

### 2.6. Group comparisons

We previously found that a subset of msTBI patients have significantly poorer white matter (WM) structural and functional integrity, and poorer cognitive function (Dennis et al., 2015a; Ellis et al., 2015). Within the first months post-injury, some patients have significantly slower interhemispheric transfer time (IHTT), measured as an event-related potential (ERP), while other patients do not differ significantly from controls. This functional brain biomarker effectively separates the msTBI group into two groups – TBI-slow and TBI-normal. Longitudinal analyses suggest that disrupted WM integrity in the TBI-slow group may even be progressive (Dennis et al., 2017). The TBI-normal group, on the other hand, continues to track with the healthy controls, showing evidence of recovery. Given these pronounced group differences, we tested for differences between TBI-slow, TBI-normal, and control groups in longitudinal changes in regional brain volumes. We included 6 volunteers scanned on both scanners as control subjects. With short scan intervals, they served to determine the effect of scanner change. We tested the voxel-wise Jacobian maps for associations with our summary cognitive score, examining the change in summary cognitive score over time for associations with change in regional brain volume. This analysis was done separately for the msTBI and control groups.

### 2.7. Statistical analysis

In our voxel-wise linear regression testing for group differences, we included intracranial volume (ICV) as a covariate. The 9 DOF linear registration that is part of our processing protocol accounts for differences in overall brain scale, removing much of the effect of ICV, but we still included ICV, computed from the linearly registered image, as a covariate. For investigating group differences, we run voxel-wise linear regression in the form:

$$X \sim A + \beta_{group} Group + \beta_{age} Age + \beta_{sex} Sex + \beta_{scan-ch} Scan - ch$$
$$+ \beta_{interval} Interval + \beta_{ICV} ICV + \varepsilon$$

where $X$ is the Jacobian determinant value at a given position, $A$ is the constant Jacobian determinant term, the βs are the covariate regression coefficients, and $\varepsilon$ is an error term. In this regression, we are including covariates for age, sex, whether the patient switched scanners between time 1 and time 2 (binary variable), the interval between time 1 and time 2 (in weeks), and ICV. Group is a binary dummy variable. There was no significant group difference in SES (socioeconomic status) so it was not included in the main model ($p = 0.19$). However, the TBI-slow group had a slightly lower average SES than the other two groups, so we also ran models comparing TBI-slow to healthy controls and TBI-slow to TBI-normal including SES as supplementary analyses. These results were largely consistent with the main model (Supplementary Table 1 and Supplementary Table 2).

The cognitive analysis was run with a similar model as above, with

**Table 2**

Differences between TBI-slow and controls and between TBI-normal and controls in longitudinal regional volume changes. For each cluster, the size (in voxels), coordinates of cluster peak (MNI), hemisphere, and tissue type are listed. "Avg. ch." is the percent volume change from the group-averaged jacobian determinant averaged across the cluster, to indicate the direction and magnitude of the change within the group. CC = corpus callosum, ec/ex/cl = external capsule/extreme capsule/claustrum, PTR = posterior thalamic radiation. SOG = superior occipital gyrus, MTG = middle temporal gyrus, SFG = superior frontal gyrus, POp = parietal operculum, post. cing. = posterior cingulate, MFG = middle frontal gyrus, PoG = postcentral gyrus, LOG = lateral occipital gyrus, MCP = middle cerebellar peduncle, PrG = precentral gyrus, SPL = superior parietal lobule, STG = superior temporal gyrus. Corrected for multiple comparisons using FDR ($q < 0.05$).

Control > TBI-slow

| Cluster location | Size (voxels) | MAX | Control avg. ch. | TBI-slow avg. ch | MNI coordinates (peak) | | | Side | Tissue |
|---|---|---|---|---|---|---|---|---|---|
| | | | | | X | Y | Z | | |
| Splenium | 935 | 1.22 | − 0.1% | − 3.0% | − 1 | − 30 | 19 | B | WM |
| CC | 512 | 1.12 | + 1.1% | − 3.6% | − 18 | − 44 | 25 | L | WM |
| ec/ex/cl | 410 | 1.13 | + 2.8% | − 3.9% | 33 | − 13 | 6 | R | WM |
| PTR | 197 | 1.16 | + 1.1% | − 2.9% | 31 | − 55 | 6 | R | WM |
| CC | 65 | 1.1 | + 1.1% | − 7.8% | − 10 | − 20 | 29 | L | WM |
| Hypothalamus | 45 | 1.14 | + 2.4% | − 8.8% | − 6 | − 2 | − 12 | L | GM |

Control > TBI-normal

| Cluster location | Size (voxels) | MAX | Control avg. ch | TBI-normal avg. ch | MNI coordinates (peak) | | | Side | Tissue |
|---|---|---|---|---|---|---|---|---|---|
| | | | | | X | Y | Z | | |
| SFG | 9401 | 1.57 | + 1.4% | − 8.8% | 11 | 4 | 64 | R | GM |
| SFG | 7791 | 1.53 | + 1.3% | − 10.1% | -13 | 4 | 60 | L | GM |
| SFG | 686 | 1.33 | + 2.5% | − 6.6% | − 32 | 29 | 39 | L | GM |
| POp | 626 | 1.18 | + 0.4% | − 3.3% | 49 | -26 | 18 | R | GM |
| Post. cing. | 593 | 1.26 | − 2.1% | − 6.8% | 1 | -40 | 32 | B | GM |
| Post. cing. | 370 | 1.24 | 0.0% | − 8.5% | 1 | -23 | 31 | B | GM |
| Thalamus | 360 | 1.19 | + 4.0% | − 2.9% | 13 | -18 | 18 | R | GM |
| MFG | 211 | 1.22 | + 2.2% | − 0.5% | 48 | 48 | 7 | R | GM |
| Putamen | 197 | 1.18 | − 1.3% | − 6.0% | 22 | 11 | -2 | R | GM |
| Post. cing. | 170 | 1.22 | − 0.9% | − 8.0% | 1 | -30 | 40 | B | GM |
| MTG | 162 | 1.16 | + 2.2% | − 3.6% | 65 | -28 | 0 | R | GM |
| PoG | 131 | 1.22 | − 3.9% | − 5.4% | − 36 | -35 | 55 | L | GM |
| LOG | 106 | 1.18 | − 5.9% | − 6.1% | 43 | -73 | 5 | R | GM |
| SFG | 93 | 1.26 | − 5.9% | − 6.1% | 45 | 22 | 43 | R | GM |
| Insula | 83 | 1.17 | − 0.6% | − 9.9% | − 34 | -1 | -7 | L | GM |

TBI-normal > Control

| Cluster location | Size (voxels) | MAX | Control avg. ch | TBI-normal avg. ch | MNI coordinates (peak) | | | Side | Tissue |
|---|---|---|---|---|---|---|---|---|---|
| | | | | | X | Y | Z | | |
| IC | 963 | 0.937 | − 1.5% | + 3.1% | 17 | 7 | 15 | R | WM |
| IC | 369 | 0.922 | + 0.3% | + 1.5% | − 22 | -8 | 14 | L | WM |

change in cognitive score in place of Group, and only run within groups, not across all subjects. The TBI subgroup analysis was also run with the above model, with TBI-group (slow v. control – binary dummy variable) in place of Group. We masked results to not include the cerebellum, as our scan comparison analyses revealed scanner-related bias in the intensity correction in the cerebellum.

## 3. Results

### 3.1. TBI-slow vs. control

We found several clusters of significant group differences in volume change. Areas showing positive regression *beta* values indicate greater increases in healthy controls compared to TBI-slow. In all of these clusters, TBI-slow patients showed longitudinal decreases in brain volume and healthy control children showed mostly increases in brain volume, with some regions showing small decreases. We examined the group-averaged data to confirm that this was not a case of TBI-slow patients still growing but not as quickly, which is shown in Table 2. The TBI-slow group largely showed decreased volume in WM clusters, as

well as a small cluster in the hypothalamus. These results are shown in Fig. 1. Results were corrected for multiple comparisons using searchlight FDR (Langers et al., 2007) ($q < 0.05$).

### 3.2. TBI-normal vs. control

We found more extensive differences between TBI-normal and control groups. While there were several areas where the TBI-normal group showed volume decreases, they also showed volume increases. These results are shown in Table 2 and Fig. 1. The TBI-normal group largely showed decreased volume in GM clusters, and increased volume in WM clusters. Results were corrected for multiple comparisons using searchlight FDR (Langers et al., 2007) ($q < 0.05$).

### 3.3. TBI-slow vs. TBI-normal

Within this subset with longitudinal data analyzed here, there is a non-significant age difference between TBI-normal and the other two groups. Our prior study included a larger cohort, and there were no differences in age or sex distribution between the groups (Dennis et al.,
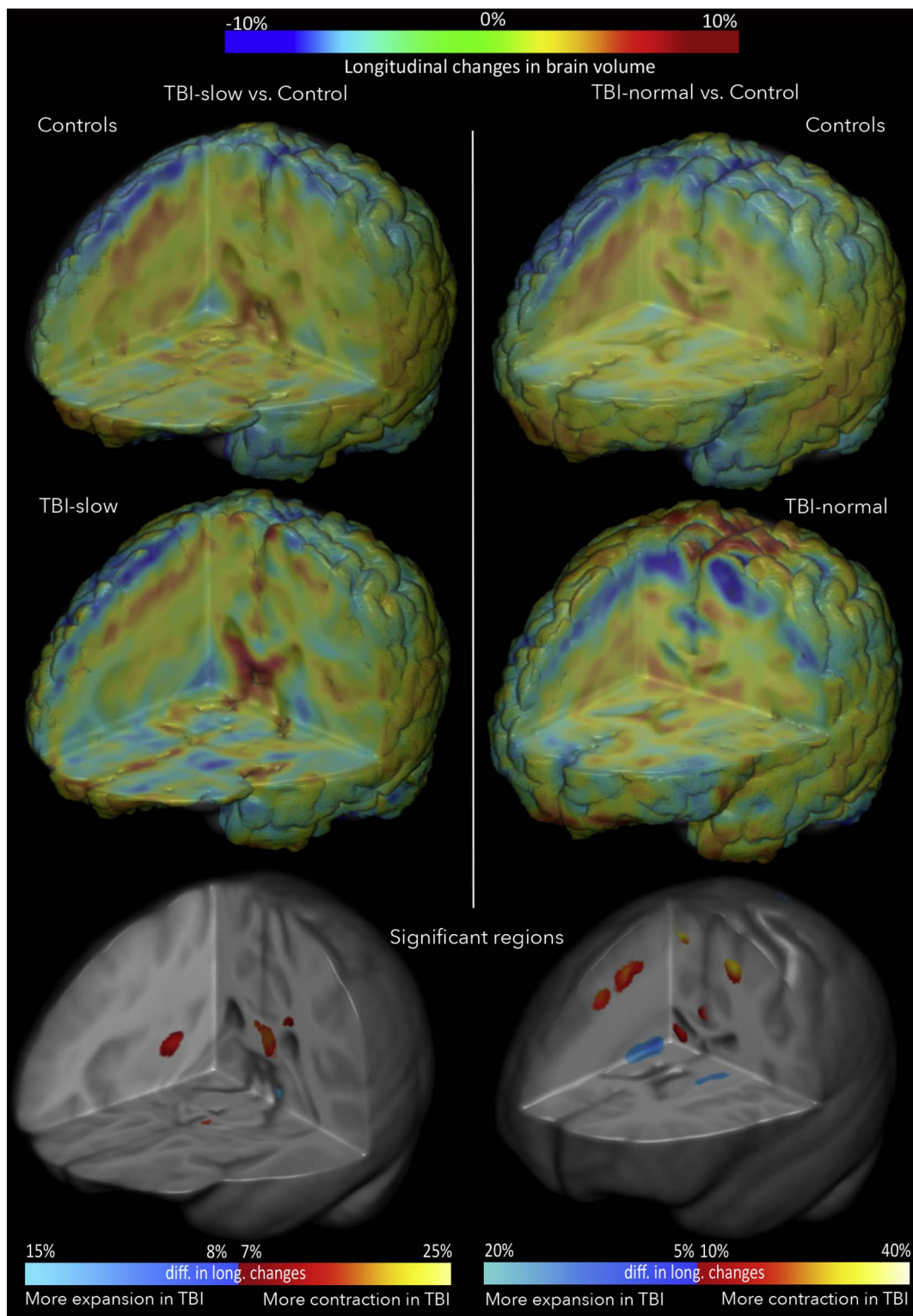
**Fig. 1.** Regional volume changes between TBI-slow and controls, and between TBI-normal and controls. Longitudinal changes in regional volume are shown for healthy controls, TBI-slow, and TBI-normal. The TBI-slow vs. control comparison is shown in the left panel, and the TBI-normal vs. control comparison is shown in the right panel. Colors in the group-averaged jacobians (top two images) represent the percent change over the 12-month interval, according to the color bar at top. Beta values are overlaid on an MDT (minimal deformation template) from the healthy controls, with beta values colored according to the color bar at bottom. Blue areas are those with greater increases in the TBI-slow or TBI-normal groups, relative to healthy controls, red-yellow areas are those with greater increases in the healthy controls, relative to the TBI groups. Left in image is right in brain.

2015a). Therefore, age differences are unlikely to account for the differences between TBI-slow and TBI-normal. In our longitudinal analyses, the inter-scan interval was consistent and we covaried for age in all analyses. When we compared longitudinal volume changes between TBI-slow and TBI-normal we found that the TBI-normal group

had volume expansion in the bilateral internal capsule (IC), overlapping with the thalamus in the right hemisphere, while the TBI-slow group showed volume reduction in these areas. There were several other clusters of significant group differences, detailed in Table 3 and Fig. 2. Results were corrected for multiple comparisons using searchlight FDR

**Table 3**

Differences between TBI-slow and TBI-normal in longitudinal regional volume changes. For each cluster, the size (in voxels), coordinates of cluster peak (MNI), hemisphere, and tissue type are listed. "Avg. ch." is the percent volume change from the group-averaged jacobian determinant averaged across the cluster, to indicate the direction and magnitude of the change within the group. IC = internal capsule, PTR = posterior thalamic radiation, SCR = superior corona radiata, MTG = middle temporal gyrus, STG = superior temporal gyrus, CP = cerebellar peduncle, SFG = superior frontal gyrus, SPL = superior parietal lobule, IOG = inferior occipital gyrus, MFG = middle frontal gyrus, POp = parietal operculum. Coordinates in MNI, left in image is right in brain. Corrected for multiple comparisons using FDR ($q < 0.05$).

**TBI-normal > TBI-slow**

| Cluster location | Size (voxels) | MAX | TBI-slow avg. ch | TBI-normal avg. ch | MNI coordinates (peak) | | | Side | Tissue |
|---|---|---|---|---|---|---|---|---|---|
| | | | | | X | Y | Z | | |
| IC/thalamus | 1015 | 1.14 | − 3.2% | + 2.3% | 24 | − 21 | 14 | R | GM/WM |
| IC | 305 | 1.14 | − 4.5% | + 1.8% | − 24 | − 23 | 13 | L | WM |
| SCR | 58 | 1.09 | − 0.2% | + 4.2% | 26 | 18 | 26 | R | WM |

**TBI-normal < TBI-slow**

| Cluster location | Size (voxels) | MAX | TBI-slow avg. ch | TBI-normal avg. ch | MNI coordinates (peak) | | | Side | Tissue |
|---|---|---|---|---|---|---|---|---|---|
| | | | | | X | Y | Z | | |
| SFG | 1262 | 0.846 | + 1.2% | − 7.5% | 27 | 30 | 45 | R | GM |
| IOG | 412 | 0.882 | − 0.8% | − 7.1% | 44 | − 65 | − 2 | R | GM/WM |
| SPL | 343 | 0.825 | + 2.6% | − 0.8% | 26 | − 60 | 49 | R | GM |
| SFG | 272 | 0.898 | + 1.4% | − 8.0% | − 25 | 30 | 33 | L | GM |
| Cingulate | 173 | 0.905 | + 2.1% | − 5.6% | 5 | − 21 | 31 | B | GM |
| MFG | 142 | 0.836 | − 2.2% | − 9.5% | − 26 | 22 | 46 | L | GM |
| SFG | 128 | 0.83 | − 2.2% | − 4.1% | − 6 | 27 | 51 | L | GM |
| Cingulate | 70 | 0.893 | − 1.5% | − 7.2% | − 6 | − 6 | 43 | L | GM |
| Cuneus | 68 | 0.808 | − 1.5% | − 5.1% | 5 | − 81 | 15 | R | GM |
| Precuneus | 54 | 0.777 | + 0.9% | − 5.9% | − 8 | − 58 | 61 | L | GM |
| POp (parietal operculum) | 51 | 0.895 | + 1.1% | − 3.6% | 51 | − 20 | 16 | R | GM |
| SFG | 47 | 0.865 | + 3.7% | + 3.2% | 24 | 44 | 35 | R | GM |

(Langers et al., 2007) ($q < 0.05$). Given the significant group differences in the IC, we additionally charted the volume of the right IC at both time points across participants in all 3 groups, shown in Fig. 3.

### 3.4. Relationships to cognitive performance

We also found widespread significant associations between regional volume changes and changes in cognitive performance. For this analysis we examined msTBI and controls separately, as we were interested to see how differences in cognitive recovery in msTBI tracked with neural recovery. We did not find significant associations between volume change and cognitive performance change in the healthy controls. We used an age-adjusted cognitive score, so associations with brain measures might not be expected in normed data from a typically developing cohort. In children with msTBI we found a number of areas positively associated with cognitive change, where increases in volume correlated with increases in cognitive performance. We also found areas where volume increases were correlated with decreases in cognitive function, or decreases in volume were correlated with increases in cognitive function, which was unexpected. While the increases were somewhat balanced between gray matter (GM) and white matter (WM), the volume decreases associated with increases in cognitive performance were largely in the GM. These results are summarized in Table 4 and Fig. 4. Results were corrected for multiple comparisons using searchlight FDR (Langers et al., 2007) ($q < 0.05$).

### 4. Discussion

In this study, we examined longitudinal changes in regional brain volume over the first 18 months post-TBI. When comparing TBI-slow vs. controls, we found atrophy in the corpus callosum (especially splenium), hypothalamus, and several other GM and WM clusters. When comparing TBI-normal vs. controls, we found volume increases in the internal capsule, and decreases across numerous GM clusters, including

subcortical regions. When comparing TBI-slow vs. TBI-normal, the internal capsule emerged as a region of greatest difference. Our results suggest that these two groups continue to diverge, with one showing longitudinal *atrophy*, the other showing signs of recovery.

Effects of msTBI on the structure, function, and metabolism of the corpus callosum (CC) have been documented for years (Babikian et al., 2010; Levin et al., 2000; Wu et al., 2010). Smaller callosal volume, disrupted tract integrity, and impaired functioning post-TBI all converge to indicate that the largest WM bundle in the brain is especially vulnerable to msTBI, and this in turn is linked with impaired cognitive function (Ewing-Cobbs et al., 2008). Our results indicate that in a significant number of patients, CC disruption not only continues but progresses over the first 18 months post-injury. While the CC of healthy controls increased in volume over this year, TBI-slow patients showed a decrease in CC volume, suggesting continued degeneration. This effect could be exaggerated by the male/female balance of the groups – the control group was 58% male while the TBI-slow group was 73% male, and studies have shown sex-specific growth patterns in the corpus callosum (Luders et al., 2010). We have found that the functional integrity of the CC 2–5 months post-injury is linked with poor CC structural integrity (Dennis et al., 2015a), but further we have found that this biomarker predicts longitudinal changes in CC integrity (Dennis et al., 2017). MsTBI patients with poor CC functional integrity 2–5 months post-injury show widespread longitudinal WM degeneration, while patients with functionally intact CC show longitudinal recovery of WM integrity. Again, these msTBI groups do not differ significantly demographically or clinically. Here we further show that CC functional integrity 2–5 months post-injury predicts tissue atrophy longitudinally.

The cingulum, the white matter bundle running perpendicular and superior to the CC, is also a common site for disruption. Prior studies found impaired white matter integrity and decreased volume in the cingulum, in both cross-sectional and longitudinal analyses (Bendlin et al., 2008). Volume changes in the overlying cingulate gyrus have also
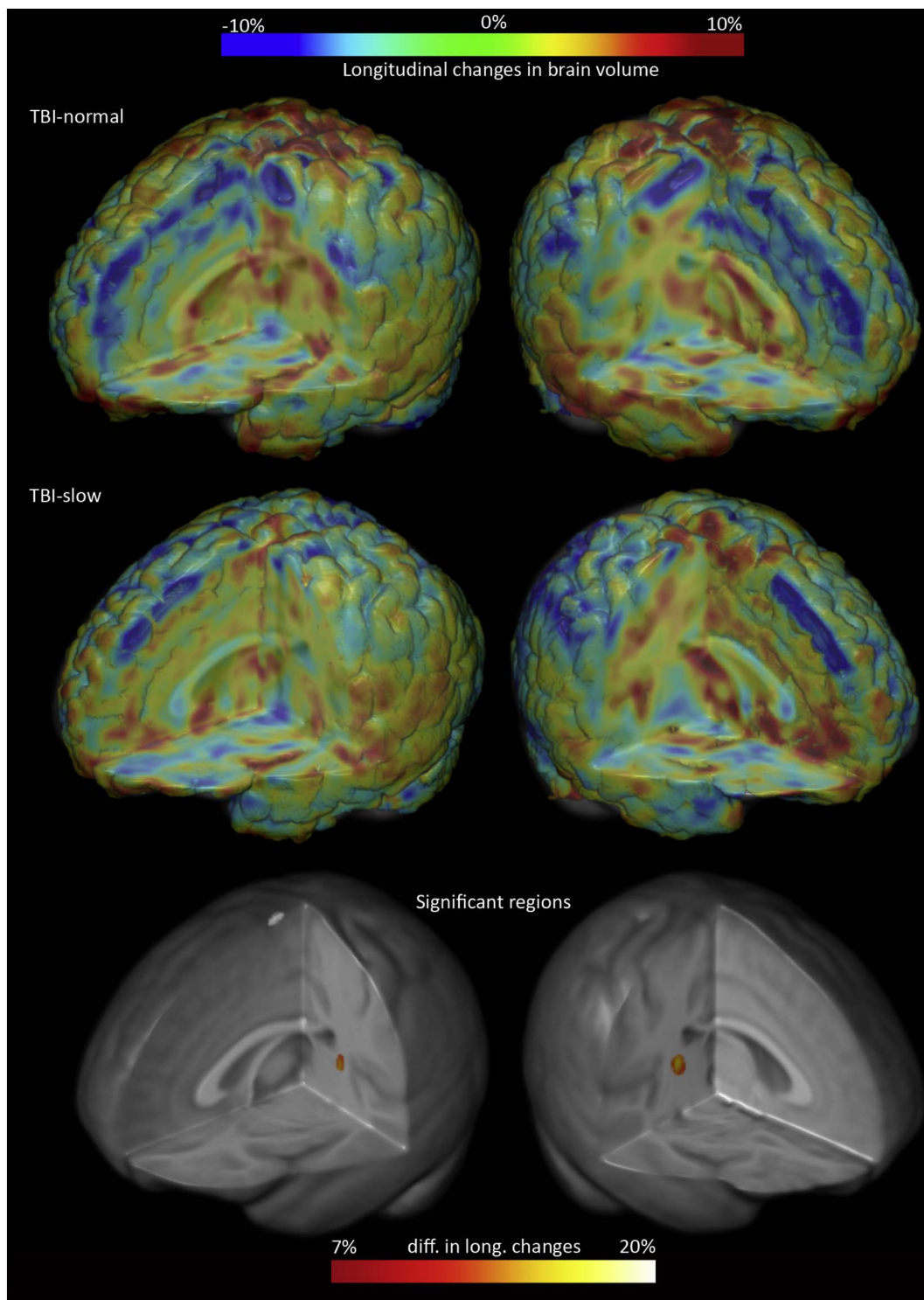
**Fig. 2.** Longitudinal regional volume changes in TBI-slow and TBI-normal groups. Longitudinal changes in regional volume are shown for the TBI-slow and TBI-normal groups. Colors in the group-averaged jacobians (top two images) represent the percent change over the 12-month interval, according to the color bar at top. Beta values are overlaid on an MDT (minimal deformation template) from the healthy controls, with beta values colored according to the color bar at bottom. Red-yellow areas shown are those with longitudinal increases in TBI-normal and decreases in TBI-slow. Left hemisphere is shown on left in image, right hemisphere on the right. (For interpretation of the references to color in this figure legend, the reader is referred to the web version of this article.)

been found and are associated with cognitive deficits (Bendlin et al., 2008). We found decreased volume longitudinally in the cingulate in TBI-normal group relative to healthy controls. As a key structure in the limbic system, disruption of the cingulum could underlie memory deficits common after injury, as well as emotional disturbances.

The putamen, thalamus, and middle cerebellar peduncle are all components of the motor system, and all showed volumes decreases in the TBI-normal group. While not tested in this cohort, motor disturbances are well-documented even in mild TBI (Kuhtz-Buschbeck et al., 2003). The integrity of the cerebellar peduncle in the post-acute phase is a good predictor of outcome one year later (Sidaros et al., 2009). The functions of the thalamus extend far beyond motor coordination. As a
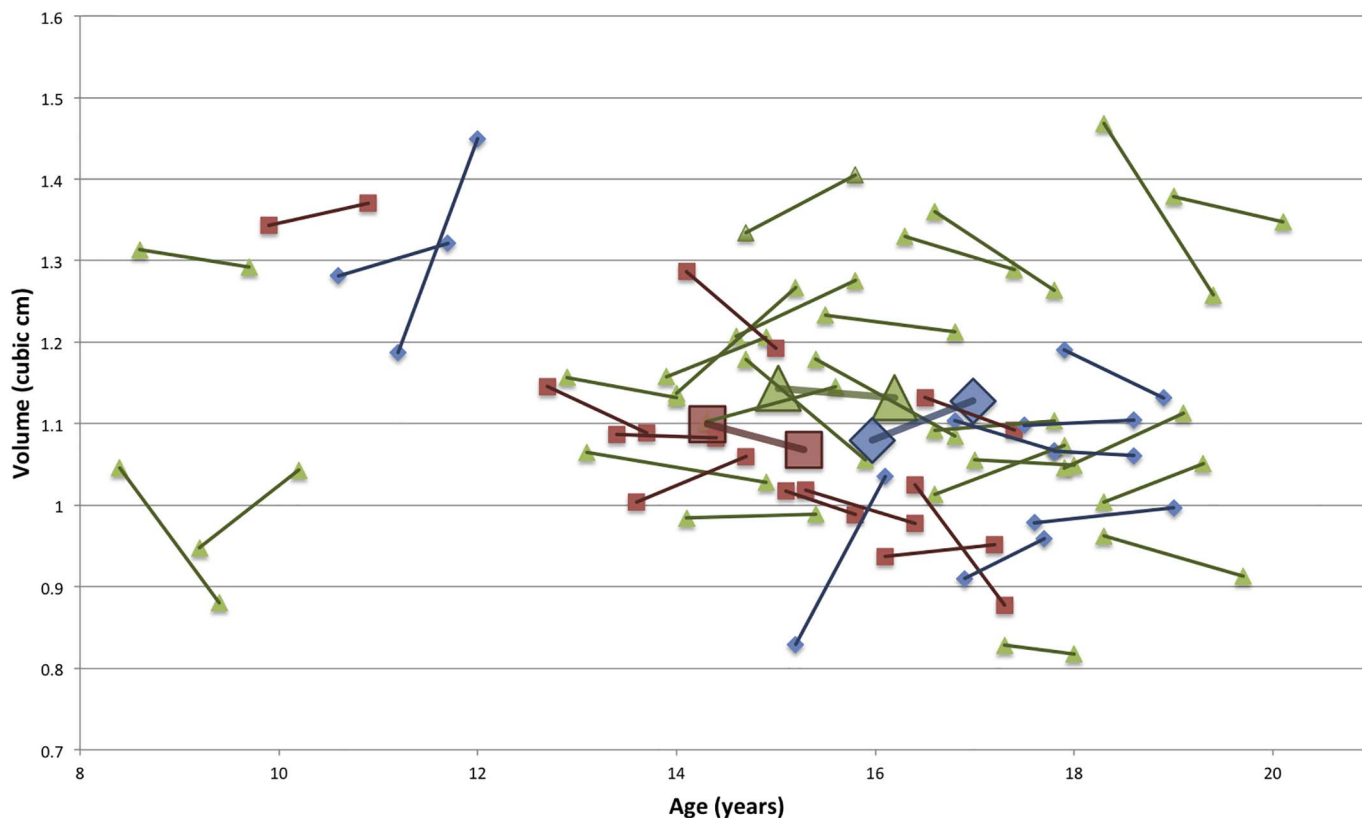
**Fig. 3.** Longitudinal changes in right internal capsule across groups. We chart the volume of the right internal capsule at both time points across control, TBI-normal, and TBI-slow groups. Age (in years) is on the X-axis, and volume (in cm³) is on the Y-axis. Green triangles indicate control participants, blue diamonds indicate TBI-normal participants, and red squares indicate TBI-slow participants, as indicated in the legend. The colored lines connect time 1 and time 2 measurements for a given participant. The larger shapes represent the average values for each of the 3 groups, with average trendlines drawn out across the scatterplot. (For interpretation of the references to color in this figure legend, the reader is referred to the web version of this article.)

relay station in the brain it also plays a role in arousal, sensory relay, and language functions (Crosson, 1985). We found decreased volume in TBI-normal in the putamen, thalamus, and MCP. However, for another component of the motor system, the internal capsule, the TBI-normal group showed volume increases relative to both the healthy controls and the TBI-slow group.

The hypothalamus is a key component of the endocrine system, synthesizing and releasing hormones via the pituitary. Neuroendocrine dysfunction has also been recognized following TBI in pediatric patients, although research has mostly focused on the pituitary. The prevalence of pituitary dysfunction increases in more severe TBI (Bondanelli et al., 2004). The most commonly disrupted hormone is growth hormone, but gonadotropins, adrenocorticotropic hormone, thyroid-stimulating hormone, and prolactin have been reportedly disrupted in patients (Rose and Auble, 2012). These can affect development and puberty. Direct studies of structural damage to the hypothalamus and pituitary are few (Acerini and Tasker, 2007). As small structures, most standard MRI sequences have poor resolution for accurate measurements of pituitary and hypothalamic volume. While we detected differences between TBI-slow and healthy controls in the longitudinal volume changes of the hypothalamus, our protocol did not require outlining these structures. In the future a specialized scan sequence focused on this region may better document how TBI affects neuroendocrine structures.

We found that our previously established groups, based on IHTT, identified TBI patients with distinct longitudinal trajectories, both relative to healthy controls and relative to each other. The TBI-slow group showed atrophy in WM structures, most notably the splenium, as well as the hypothalamus. The areas of decreased volume in the TBI-normal group included entirely GM structures, while they showed increased volume in WM structures. This could be a sign of atrophy, in

subcortical structures and throughout the cerebrum, but another consideration is that these children are still developing. Countless studies document decreases in GM volume and density over development, as connections are pruned and intracortical myelination continues (Dennis and Thompson, 2013; Gogtay et al., 2004). As GM volume decreases are developmentally expected, it is possible that these are indications of a return to a healthy developmental trajectory in some of our patients. This could also be due to the age difference between the TBI-normal group and others, although this was not significant. It could also be that we have identified two subtypes of pathology – one primarily marked by decreases in WM integrity and volume, and the other where the WM is spared and the GM shows pathology.

When we examined cognitive correlates of changes in brain volume in the msTBI patients, we found both positive and negative correlations, with changes in WM regions generally positively associated with changes in cognitive function, and changes in GM regions generally negatively associated. Increasing volume with increasing cognitive function can be interpreted as signs of recovery, as WM tracts are myelinated to support cognitive development (Kochunov et al., 2010). Decreases in GM volume that correlate with increases in cognitive function could reflect some patients returning to a typical developmental trajectory. Another consideration with these results is that we are looking at changes in a cognitive score that is normalized by age. So "decreases" in age-normalized cognitive score associated with increases in volume do not necessarily indicate decreases in the raw cognitive scores. Subjects with a "decreased" performance score may just have not kept pace with the developmentally expected outcome.

There is considerable heterogeneity in TBI – in injury severity, location, type, and countless peripheral factors that may affect outcome. It is therefore critical, especially in longitudinal analyses, to have

**Table 4**

Associations between cognitive performance change and regional volume change in the msTBI group. For each cluster, the size (in voxels), effect size (the % change in volume associated with a 1 point increase in cognitive score), coordinates of cluster peak (MNI), hemisphere, and tissue type are listed. MFG = middle frontal gyrus, SFG = superior frontal gyrus, PPo = planum polare, PTe = planum temporale, SOG = superior occipital gyrus, CR = corona radiata, MTG = middle temporal gyrus, IFG = inferior frontal gyrus, SPL = superior parietal lobule, ITG = inferior temporal gyrus, MOG = middle occipital gyrus, IC = internal capsule, STG = superior temporal gyrus, LOG = lateral occipital gyrus, Corrected for multiple comparisons using FDR ($q < 0.05$).

Positive associations between volume change and cognitive change

| Cluster location | Size (voxel) | Max. effect | MNI coordinates (peak) | | | Side | Tissue |
|---|---|---|---|---|---|---|---|
| | | | X | Y | Z | | |
| MFG | 7961 | 3.4% | 40 | 63 | − 1 | R | GM |
| MFG | 2787 | 3.3% | − 33 | 64 | − 7 | L | GM |
| Fusiform G | 2777 | 1.7% | − 30 | − 70 | − 12 | L | WM |
| SFG | 1221 | 3.0% | − 8 | 71 | 23 | L | GM |
| Cingulate G | 539 | 1.5% | − 12 | − 55 | 15 | L | WM |
| Genu | 295 | 1.4% | 14 | 25 | 9 | R | WM |
| PPo | 253 | 2.5% | − 20 | 19 | − 33 | L | GM |
| Supramarginal G | 210 | 2.0% | − 57 | − 47 | 51 | L | GM |
| PTe | 203 | 1.3% | 47 | − 31 | 16 | R | GM |
| Insula | 184 | 1.7% | 35 | 14 | − 17 | R | GM |
| SOG | 166 | 0.8% | 25 | − 57 | 23 | R | WM |
| Cuneus | 139 | 1.7% | 15 | − 94 | 1 | R | GM |
| CR | 122 | 1.0% | − 20 | 1 | 34 | L | WM |
| Genu | 104 | 0.9% | − 15 | 28 | 11 | L | WM |
| SFG | 84 | 1.1% | − 46 | 42 | 16 | L | GM |
| MTG | 59 | 1.0% | − 50 | − 51 | − 2 | L | WM |
| IFG | 59 | 1.2% | − 37 | 28 | 0 | L | GM |
| SPL | 53 | 1.6% | 31 | − 50 | 52 | R | GM |

Negative associations between volume change and cognitive change

| Cluster location | Size (voxel) | Max. effect | MNI coordinates (peak) | | | Side | Tissue |
|---|---|---|---|---|---|---|---|
| | | | X | Y | Z | | |
| SFG | 1798 | − 0.8% | 26 | 44 | 24 | R | GM/WM |
| Cuneus | 1430 | − 0.7% | − 23 | − 66 | 24 | L | GM/WM |
| Cuneus | 1066 | − 0.7% | 21 | − 68 | 14 | R | GM |
| Angular G | 1006 | − 0.5% | 45 | − 50 | 26 | R | GM |
| IOG | 791 | − 0.6% | − 57 | − 69 | − 7 | L | GM |
| IOG | 782 | − 0.4% | − 64 | − 56 | 1 | L | GM |
| Fusiform G | 739 | − 0.9% | 43 | − 36 | − 23 | R | GM |
| MOG | 714 | − 0.9% | 31 | − 75 | 24 | R | GM |
| SFG | 557 | − 0.9% | − 12 | 53 | 10 | L | GM/WM |
| CR | 551 | − 0.6% | 19 | 33 | 14 | R | WM |
| LOG | 471 | − 0.7% | − 42 | − 67 | 15 | L | GM |
| Angular G | 463 | − 0.5% | − 48 | − 54 | 20 | L | GM |
| MFG | 463 | − 0.7% | 43 | 43 | 10 | R | GM |
| SPL | 439 | − 1.3% | 18 | − 65 | 61 | R | GM |
| Cingulate G | 307 | − 0.6% | 13 | 34 | 31 | R | GM |
| Post. cingulate G | 296 | − 0.6% | 13 | − 43 | 32 | R | GM |
| Precuneus | 283 | − 0.9% | 10 | − 74 | 50 | R | GM |
| Cingulate G | 283 | − 0.6% | − 8 | 36 | 11 | L | GM |
| SOG | 254 | − 1.0% | 18 | − 90 | 19 | R | GM |
| STG | 192 | − 0.5% | − 55 | − 36 | 11 | L | GM |
| SPL | 177 | − 1.6% | 13 | − 53 | 70 | R | GM |
| IC | 151 | − 0.7% | − 18 | 20 | 5 | L | WM |
| MOG | 115 | − 1.1% | − 23 | − 91 | 10 | L | GM |
| ITG | 109 | − 0.8% | − 51 | − 45 | − 23 | L | GM |
| STG | 99 | − 0.8% | − 54 | − 12 | − 12 | L | GM |
| Fusiform G | 99 | − 0.9% | − 39 | − 34 | − 23 | L | GM |
| Angular G | 84 | − 1.0% | 37 | − 50 | 41 | R | GM |
| Genu | 77 | − 0.7% | − 9 | 28 | 0 | L | WM |
| SMG | 69 | − 0.7% | − 62 | − 31 | 27 | L | GM |
| Genu | 58 | − 0.7% | 11 | 26 | 0 | R | WM |
| Insula | 56 | − 0.5% | − 35 | − 24 | − 1 | L | GM |
| Fusiform G | 45 | − 1.2% | 35 | − 18 | − 32 | R | GM |
| Angular G | 42 | − 1.1% | − 32 | − 44 | 40 | L | GM |

accurate non-linear registration or results will be inaccurate. We used a study specific template, which can improve registration relative to a standard template (Hua et al., 2013) and concatenated transformations so that minimal information was lost during the resampling step. We used ANTs SyN to drive non-linear registration as it performs favorably compared to other non-linear registration algorithms (Klein et al., 2009) and is open-source. ANTs SyN, which produces topology preserving and invertible mappings between 3D images, has been shown to be
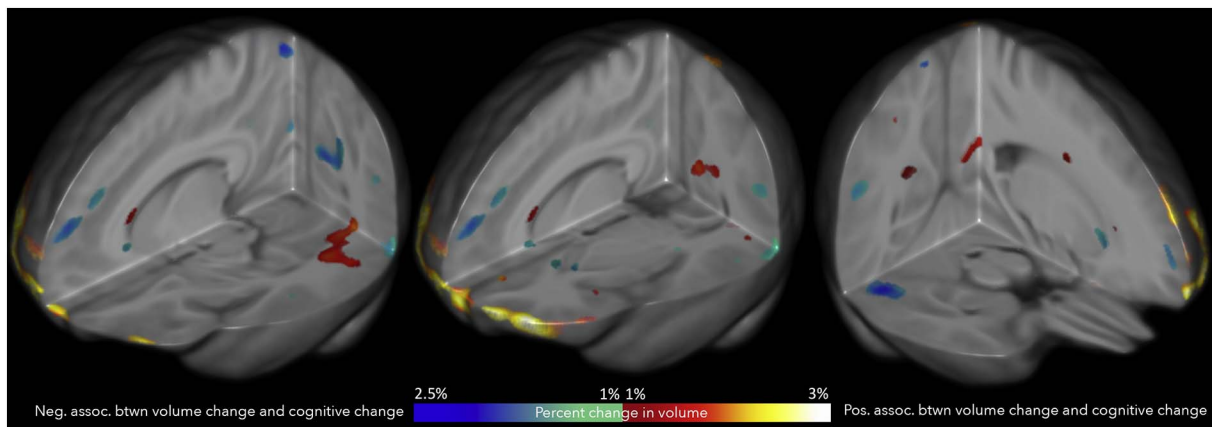
**Fig. 4.** Associations between cognitive performance change and regional volume change in the msTBI group. Yellow/red are areas where volume change was positively associated with cognitive performance change, while blue/teal areas are where volume change was negatively associated with cognitive performance change. Left in image is right in brain. Corrected for multiple comparisons using FDR ($q < 0.05$). (For interpretation of the references to color in this figure legend, the reader is referred to the web version of this article.)

effective for evaluating TBI-induced volume changes (Kim et al., 2008). There are undoubtedly patient-specific areas of volume change not detected in our analysis that may have an impact on patient functioning, but mapping patient-specific disruption is a different question from the generalizable disruptions we aimed to map here. Our sample size was relatively small, once the TBI group was separated into the subgroups. For this reason, the results we present should be considered preliminary until replication in a new sample. Another limitation is the under-representation of younger patients – although we included patients as young as 8 years old, the majority were between 13 and 17 at the time of their first scan. Additionally, our healthy control group includes more females than the TBI groups – the TBI group was 31% female, while the healthy control group was 42% female. This slight difference could cause some bias in our results, also necessitating replication in future samples. One issue that can affect all imaging studies, and could theoretically have a larger impact in longitudinal studies, is the test-retest reliability of volume estimates due to differences in hydration and time of day (Maclaren et al., 2014). We would not expect this factor to introduce systematic bias across the sample, however.

## 5. Conclusions

We present longitudinal results showing distinct longitudinal trajectories in two subgroups of msTBI patients. We linked volume changes to changes in cognitive function in the msTBI group, suggesting delayed maturation in some patients. The first 18 months post-injury are a dynamic period, and post-injury outcomes vary widely. The ability to use early electrophysiological and imaging measures to predict trajectories in brain development has the potential to provide extremely valuable information clinically. These early biomarkers may suggest mechanism-specific interventions that can improve longer-term function and neural integrity, or at a minimum, serve as prognostic markers in the complex process of understanding pediatric/adolescent TBI outcomes.

## Conflict of interest

Dr. Giza reports consultant fees from NFL-Neurological Care Program, NHLPA, Neural Analytics, serves on the advisory panel for the Major League Soccer, NCAA, US Soccer Federation, and has received speaker fees from Medical Education Speakers Network.

## Appendix A. Supplementary data

Supplementary data to this article can be found online at http://dx.doi.org/10.1016/j.nicl.2017.03.014.

## References

Acerini, C.L., Tasker, R.C., 2007. Traumatic brain injury induced hypothalamic-pituitary dysfunction: a paediatric perspective. Pituitary 10, 373–380.

Avants, B.B., Epstein, C.L., Grossman, M., Gee, J.C., 2008. Symmetric diffeomorphic image registration with cross-correlation: evaluating automated labeling of elderly and neurodegenerative brain. Med. Image Anal. 12, 26–41.

Avants, B.B., Tustison, N.J., Song, G., Cook, P.A., Klein, A., Gee, J.C., 2011. A reproducible evaluation of ANTs similarity metric performance in brain image registration. NeuroImage 54, 2033–2044.

Babikian, T., Asarnow, R., 2009. Neurocognitive outcomes and recovery after pediatric TBI: meta-analytic review of the literature. Neuropsychology 23, 283–296.

Babikian, T., Marion, S.D., Copeland, S., Alger, J.R., O'Neill, J., Cazalis, F., Mink, R., Giza, C.C., Vu, J.A., Hilleary, S.M., 2010. Metabolic levels in the corpus callosum and their structural and behavioral correlates after moderate to severe pediatric TBI. J. Neurotrauma 27, 473–481.

Bendlin, B.B., Ries, M.L., Lazar, M., Alexander, A.L., Dempsey, R.J., Rowley, H.A., Sherman, J.E., Johnson, S.C., 2008. Longitudinal changes in patients with traumatic brain injury assessed with diffusion-tensor and volumetric imaging. NeuroImage 42, 503–514.

Bondanelli, M., De Marinis, L., Ambrosio, M.R., Monesi, M., Valle, D., Zatelli, M.C., Fusco, A., Bianchi, A., Farneti, M., degli Uberti, E.C., 2004. Occurrence of pituitary dysfunction following traumatic brain injury. J. Neurotrauma 21, 685–696.

Crosson, B., 1985. Subcortical functions in language: a working model. Brain Lang. 25, 257–292.

Delis, D.C., Kaplan, E., Kramer, J.H., 2001. Delis-Kaplan Executive Function System (D-KEFS). Psychological Corporation.

Delis, D.C., Kramer, J.H., Kaplan, E., Ober, A., 1994. California Verbal Learning Test-children's Version (CVLT-C). Springer, New York, NY.

Dennis, E.L., Thompson, P.M., 2013. Typical and atypical brain development: a review of neuroimaging studies. Dialogues Clin. Neurosci. 15, 359–383.

Dennis, E.L., Rashid, F., Ellis, M.U., Babikian, T., Villalon-Reina, J.E., Jin, Y., Olsen, A., Mink, R., Babbitt, C., Johnson, J., Giza, C.C., Thompson, P.M., Asarnow, R.F., 2017. Progressive white matter damage in pediatric moderate/severe traumatic brain injury: A longitudinal study. Neurology Published online before print March 15, 2017. http://dx.doi.org/10.1212/WNL.0000000000003808.

Dennis, E.L., Ellis, M.U., Marion, S.D., Jin, Y., Moran, L., Olsen, A., Kernan, C., Babikian,

T., Mink, R., Babbitt, C., Johnson, J., Giza, C.C., Thompson, P.M., Asarnow, R.F., 2015a. Callosal function in pediatric traumatic brain injury linked to disrupted white matter integrity. J. Neurosci. 35, 10202–10211.

Dennis, E.L., Jin, Y., Villalon-Reina, J., Zhan, L., Kernan, C., Babikian, T., Mink, R., Babbitt, C., Johnson, J., Giza, C.C., 2015b. White matter disruption in moderate/severe pediatric traumatic brain injury: advanced tract-based analyses. NeuroImage: Clinical 7, 493–505.

Dennis, E.L., Hua, X., Villalon-Reina, J., Moran, L.M., Kernan, C., Babikian, T., Mink, R., Babbitt, C., Johnson, J., Giza, C.C., Thompson, P.M., Asarnow, R.F., 2015. Tensor-based morphometry reveals volumetric deficits in moderate/severe pediatric traumatic brain injury. J. Neurotrauma 33 (9), 840–852.

Ellis, M.U., Marion, S.D., McArthur, D.L., Babikian, T., Giza, C., Kernan, C.L., Newman, N., Moran, L., Akarakian, R., Houshiarnejad, A., Mink, R., Johnson, J., Babbitt, C.J., Olsen, A., Asarnow, R.F., 2015. The UCLA study of children with moderate-to-severe traumatic brain injury: event-related potential measure of interhemispheric transfer time. J. Neurotrauma (In Press).

Ewing-Cobbs, L., Prasad, M.R., Swank, P., Kramer, L., Cox, J., Charles, S., Fletcher, J.M., Barnes, M., Zhang, X., Hasan, K.M., 2008. Arrested development and disrupted callosal microstructure following pediatric traumatic brain injury: relation to neurobehavioral outcomes. NeuroImage 42, 1305–1315.

Farbota, K.D., Sodhi, A., Bendlin, B.B., McLaren, D.G., Xu, G., Rowley, H.A., Johnson, S.C., 2012. Longitudinal volumetric changes following traumatic brain injury: a tensor-based morphometry study. J. Int. Neuropsychol. Soc. 18, 1006–1018.

Gogtay, N., Giedd, J.N., Lusk, L., Hayashi, K.M., Greenstein, D., Vaituzis, A.C., Nugent III, T.F., Herman, D.H., Clasen, L.S., Toga, A.W., Rapaport, J.L., Thompson, P.M., 2004. Dynamic mapping of human cortical development during childhood through early adulthood. PNAS 101, 8174–8179.

Hua, X., Ching, C.R., Mezher, A., Gutman, B.A., Hibar, D.P., Bhatt, P., Leow, A.D., Jack, C.R., Bernstein, M.A., Weiner, M.W., 2016. MRI-based brain atrophy rates in ADNI phase 2: acceleration and enrichment considerations for clinical trials. Neurobiol. Aging 37, 26–37.

Hua, X., Hibar, D.P., Ching, C.R., Boyle, C.P., Rajagopalan, P., Gutman, B.A., Leow, A.D., Toga, A.W., Jack Jr., C.R., Harvey, D., Weiner, M.W., Thompson, P.M., Alzheimer's Disease Neuroimaging, I., 2013. Unbiased tensor-based morphometry: improved robustness and sample size estimates for Alzheimer's disease clinical trials. NeuroImage 66, 648–661.

Hua, X., Leow, A.D., Levitt, J.G., Caplan, R., Thompson, P.M., Toga, A.W., 2009. Detecting brain growth patterns in normal children using tensor-based morphometry. Hum. Brain Mapp. 30, 209–219.

Hua, X., Leow, A.D., Parikshak, N., Lee, S., Chiang, M.-C., Toga, A.W., Jack Jr., C.R., Weiner, M.W., Thompson, P.M., 2008. Tensor-based morphometry as a neuroimaging biomarker for Alzheimer's disease: an MRI study of 676 AD, MCI, and normal subjects. NeuroImage 43, 458–469.

Keenan, H.T., Bratton, S.L., 2006. Epidemiology and outcomes of pediatric traumatic brain injury. Dev. Neurosci. 28, 256–263.

Kim, J., Avants, B., Patel, S., Whyte, J., Coslett, B.H., Pluta, J., Detre, J.A., Gee, J.C., 2008. Structural consequences of diffuse traumatic brain injury: a large deformation tensor-based morphometry study. NeuroImage 39, 1014–1026.

Klein, A., Andersson, J., Ardekani, B.A., Ashburner, J., Avants, B., Chiang, M.C.,

Christensen, G.E., Collins, D.L., Gee, J., Hellier, P., Song, J.H., Jenkinson, M., Lepage, C., Rueckert, D., Thompson, P., Vercauteren, T., Woods, R.P., Mann, J.J., Parsey, R.V., 2009. Evaluation of 14 nonlinear deformation algorithms applied to human brain MRI registration. NeuroImage 46, 786–802.

Kochunov, P., Williamson, D.E., Lancaster, J., Fox, P., Cornell, J., Blangero, J., Glahn, D.C., 2010. Fractional anisotropy of water diffusion in cerebral white matter across the lifespan. Neurobiol. Aging 1–12.

Kuhtz-Buschbeck, J.P., Stolze, H., Golge, M., Ritz, A., 2003. Analyses of gait, reaching, and grasping in children after traumatic brain injury. Arch. Phys. Med. Rehabil. 84, 424–430.

Langers, D.R., Jansen, J.F., Backes, W.H., 2007. Enhanced signal detection in neuroimaging by means of regional control of the global false discovery rate. NeuroImage 38, 43–56.

Levin, H.S., Benavidez, D.A., Verger-Maestre, K., Perachio, N., Song, J., Mendelsohn, D.B., Fletcher, J.M., 2000. Reduction of corpus callosum growth after severe traumatic brain injury in children. Neurology 54, 647–653.

Luders, E., Thompson, P.M., Toga, A.W., 2010. The development of the corpus callosum in the healthy human brain. J. Neurosci. 30, 10985–10990.

Maclaren, J., Han, Z., Vos, S.B., Fischbein, N., Bammer, R., 2014. Reliability of brain volume measurements: a test-retest dataset. Sci. Data 1, 140037.

Moran, L.M., Babikian, T., Del Piero, L., Ellis, M.U., Kernan, C.L., Newman, N., Giza, C.C., Mink, R., Johnson, J., Babbitt, C., Asarnow, R., 2016. The UCLA study of predictors of cognitive functioning following moderate/severe pediatric traumatic brain injury. J. Int. Neuropsychol. Soc. 22 (05), 512–519 (Vancouver).

Rose, S.R., Auble, B.A., 2012. Endocrine changes after pediatric traumatic brain injury. Pituitary 15, 267–275.

Saatman, K.E., Duhaime, A.-C., Bullock, R., Maas, A.I.R., Valadka, A., Manley, G.T., 2008. Classification of traumatic brain injury for targeted therapies. J. Neurotrauma 25, 719–738.

Sidaros, A., Skimminge, A., Liptrot, M.G., Sidaros, K., Engberg, A.W., Herning, M., Paulson, O.B., Jernigan, T.L., Rostrup, E., 2009. Long-term global and regional brain volume changes following severe traumatic brain injury: a longitudinal study with clinical correlates. NeuroImage 44, 1–8.

Teasdale, G., Murray, G., Parker, L., Jennett, B., 1979. Adding up the Glasgow coma score. In: Proceedings of the 6th European Congress of Neurosurgery. Springer, pp. 13–16.

Thompson, P.M., Giedd, J.N., Woods, R.P., MacDonald, D., Evans, A., Toga, A., 2000. Growth patterns in the developing brain detected by using continuum mechanical tensor maps. Nat. Lett. 404, 1–4.

Wechsler, D., 2003. Wechsler Intelligence Scale for Children–Fourth Edition (WISC-IV). Pearson, San Antonio.

Wilde, E.A., Bigler, E.D., Hunter, J.V., Fearing, M.A., Scheibel, R.S., Newsome, M.R., Johnson, J.L., Bachevalier, J., Li, X., Levin, H.S., 2007. Hippocampus, amygdala, and basal ganglia morphometrics in children after moderate-to-severe traumatic brain injury. Dev. Med. Child Neurol. 49, 294–299.

Wu, T.C., Wilde, E.A., Bigler, E.D., Li, X., Merkley, T.L., Yallampalli, R., McCauley, S.R., Schnelle, K.P., Vasquez, A.C., Chu, Z., Hanten, G., Hunter, J.V., Levin, H.S., 2010. Longitudinal changes in the corpus callosum following pediatric traumatic brain injury. Dev. Neurosci. 32, 361–373.